OE Optical Engineering

RESEARCH PAPER

Shock-wave tolerant phase reconstruction algorithm for Shack–Hartmann wavefront sensor data

Thomas E. DeFoor,[a,*] Matthew Kalensky,[b] Matthew R. Kemnetz,[c] Timothy J. Bukowski,[b] and Mark F. Spencer[d]

[a]The Ohio State University, College of Engineering, Columbus, Ohio, United States
[b]Naval Surface Warfare Center Dahlgren Division, Integrated Engagement Systems Department, Dahlgren, Virginia, United States
[c]Directed Energy Directorate, Air Force Research Laboratory, Kirtland Air Force Base, New Mexico, United States
[d]Air Force Institute of Technology, Department of Engineering Physics, Wright–Patterson Air Force Base, Ohio, United States

ABSTRACT. We develop a phase reconstruction algorithm for the Shack–Hartmann wavefront sensor (SHWFS) that is tolerant to phase discontinuities, such as the ones imposed by shock waves. In practice, this algorithm identifies SHWFS locations where the resultant tilt information is affected by the shock and improves the tilt information in these locations using the local SHWFS observation-plane irradiance patterns. The algorithm was shown to work well over the range of conditions tested with both simulated and experimental data. In turn, the reconstruction algorithm will enable robust wavefront sensing in transonic, supersonic, and hypersonic environments.

Keywords: aero-optics; aero-effects; shock waves; wavefront sensing; Shack–Hartmann wavefront sensor; phase discontinuities

Paper 20230814G received Aug. 29, 2023; revised Nov. 22, 2023; accepted Nov. 28, 2023; published Dec. 20, 2023.

1 Introduction

The Shack–Hartmann wavefront sensor (SHWFS) is a common tool used to measure optical-path difference (OPD) for a variety of applications. The sensor consists of an array of lenslet sub-apertures that focus portions of the incident light onto a camera detector. Phase tilts in the sub-aperture's pupil plane manifest as irradiance patterns shifted from their on-axis locations in the observation plane. These shifts, along with the focal length of the lenslets, are then used to estimate the corresponding tilt across each sub-aperture pupil. Using a least-squares reconstructor allows these measured tilts to be used to estimate the continuous OPD.[1–3] For the purposes of this paper, all findings will be reported in terms of phase, ϕ, which can be related to OPD by $\phi = (-2\pi/\lambda) * \text{OPD}$.

It has been shown that least-squares reconstruction of SHWFS slope data struggles with correctly estimating phase when discontinuities are present within the measurement aperture.[4–8] Shock waves, such as ones that form due to locally supersonic flow, can be modeled as near-instantaneous increases in density which, consequently, result in near-instantaneous changes in the optical phase for light propagating through the shocks.

*Address all correspondence to Thomas E. DeFoor, defoor.2@osu.edu

Recent studies on the effects of aperture-intersecting shock waves on SHWFS data revealed that least-squares reconstruction yields accurate estimates of the change in phase across a shock, $|\Delta\phi|$, when the magnitude of the phase discontinuity is between 0 and approximately 0.5π rad.[9,10] When the magnitude of the phase discontinuity across the shock was greater than 0.5π rad, the shock-induced tilt across the measurement sub-apertures did not result in a proportional shift of the observation-plane irradiance pattern. Consequently, this led to an incorrect estimation of the OPD. This discrepancy was caused by the bifurcation of the irradiance pattern peaks in the observation plane resulting from the shock-induced phase discontinuity in the pupil plane. In other words, this bifurcation causes discrepancies between the pupil-plane tilt and the so-called centroid tilt (C-tilt) measured from the irradiance pattern shift in the observation plane. This behavior has also been observed experimentally.[11,12]

In the past, SHWFS data have been collected through shock waves;[13] however, the incorrect estimation of $\Delta\phi$ resulting from the sub-aperture irradiance pattern bifurcation was not addressed. The purpose of this paper is to develop a first-of-its-kind, shock-tolerant phase reconstruction algorithm for the SHWFS utilizing findings presented in Ref. 10. This algorithm shows tremendous potential in extending the usefulness of the SHWFS into optical-turbulence environments where shock waves are present. In practice, the algorithm uses the following steps:

1. Calculate the tilts for each sub-aperture in the traditional sense using SHWFS data (calculate local x and y tilts from observation-plane irradiance pattern deflections).
2. Identify sub-aperture locations affected by the shock using a beam-spread metric (identify corrupted tilt information to be replaced).
3. Calculate the angle of the shock wave relative to the SHWFS x and y axes.
4. Use the observation-plane irradiance pattern to obtain a better estimate of the local tilt across each identified sub-aperture.
5. Replace the corrupted tilt information with the new tilt information found in step 4. The tilt data are then reconstructed into a continuous phase sheet using a least-squares reconstructor.

Each of these steps are discussed in Sec. 2. Simulated and experimental data are then used to demonstrate the algorithm, the results of which are presented in Sec. 3. Section 4 summarizes the paper.

2 Approach

In this section, each step of the algorithm is described in earnest.

2.1 Traditional Tilt Calculation

The first step of this algorithm, as outlined above, is to calculate the pupil-plane tilts from the SHWFS data in the traditional sense. Here, the observation-plane irradiance pattern shifts for each sub-aperture are calculated from their on-axis position and used along with the focal length of lenslets to estimate the local pupil-plane tilts. Without any extensions, these tilts are then used in a least-squares reconstructor to estimate continuous ϕ. Hereafter, this approach will be referred to as the "traditional" approach to which the "tolerant" approach, discussed in the next few sections, will be compared.

2.2 Identify Affected Sub-Apertures

As shown in Ref. 10, when the $|\Delta\phi|$ caused by a shock wave intersecting the measurement aperture exceeds $\sim 0.5\pi$ rad, the shock-induced phase discontinuity in the pupil-plane of the SHWFS sub-aperture lenslets causes appreciable beam spreading in the resulting observation-plane irradiance patterns. Therefore, in order to identify which sub-aperture lenslets are affected by the shock, beam spread can be calculated for each of the sub-aperture observation-plane irradiance patterns. In this case, the second-moment beam width, otherwise referred to as $D4\sigma$, has proven promising. The equation for $D4\sigma$ along the x axis, $D4\sigma_x$, is given as

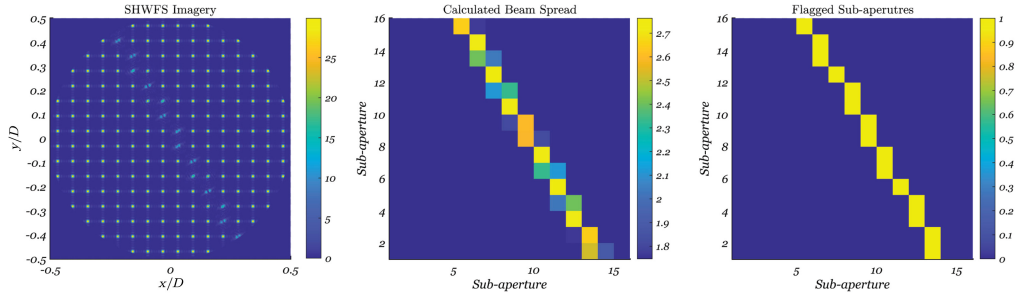

(a) (b) (c)

Fig. 1 (a) SHWFS image, (b) calculated $D4\sigma$ for sub-apertures, and (c) flagged sub-apertures for an intersecting shock of $\Delta\phi = -\pi$ and an angle 30 deg from the vertical (CCW).

$$D4\sigma_x = 4\sqrt{\frac{\sum_{i=1}^{n}(x_i - \bar{x})^2 I_i}{\sum_{i=1}^{n} I_i}}, \tag{1}$$

where n is the total number of pixels inside the sub-aperture irradiance image, I_i is the observation-plane irradiance value associated with each pixel, i, inside the sub-aperture, and $\bar{x}$ is the centroid pixel location in the x direction. Here, the sub-aperture irradiance image has been converted to a raster-ordered vector to simplify the computation of $D4\sigma_x$.[14] A similar equation can be written for $D4\sigma_y$. It is often convenient to report an overall $D4\sigma$, which can be accomplished by

$$D4\sigma = \sqrt{D4\sigma_x^2 + D4\sigma_y^2}. \tag{2}$$

Equation (2) is calculated for each sub-aperture observation-plane irradiance pattern and the results are normalized by the diffraction-limited spot size, D_{DL}. For square apertures, D_{DL} is given as $D_{\mathrm{DL}} = 2\lambda f/D$, and for circular apertures, D_{DL} is given as $D_{\mathrm{DL}} = 2.44\lambda f/D$, where λ is the wavelength of light, f is the focal length of the lenslets, and D is the diameter of the lenslets. With appropriate thresholding, affected sub-apertures can be identified—i.e., high beam spread identifies a shock-affected sub-aperture, while low beam spread does not.

To illustrate this last point, a phase discontinuity of $\Delta\phi = -\pi$ rad was applied to a simulated, uniform, complex-optical field. The phase discontinuity was at a 30 deg angle (measured counterclockwise) from the vertical and offset from the middle of the measurement aperture by half a sub-aperture diameter. This complex-optical field was then applied to an SHWFS model consisting of 16×16 sub-apertures. The resultant SHWFS imagery is shown in the leftmost plot in Fig. 1. We see that along the line where the simulated shock occurs, the associated SHWFS-irradiance patterns bifurcate. The degree of beam spreading calculated by Eq. (2) is shown in the middle plot of Fig. 1. Irradiance patterns that exhibit sufficient beam spread to qualify for being affected by the shock can be identified by thresholding the beam-spread values presented in the middle plot of Fig. 1. The flagged sub-apertures that met the thresholding criteria are presented in the rightmost plot of Fig. 1. In the sections that follow, we discuss the processing steps required to replace the corrupted tilt information in pupil locations flagged by the beam-spread calculation.

2.3 Calculate Shock Angle

After the sub-apertures affected by the shock have been identified, the angle that the shock intersects the SHWFS measurement aperture is calculated. This paper explores two methods to achieve this:

1. The first approach fits a line to the locations where the affected sub-apertures were identified. As such, this method assumes that only one shock intersects the SHWFS measurement aperture. Using a MATLAB function referred to as peaks2,[15] the two largest peaks from the observation-plane irradiance pattern were recorded. The accuracy of this method is limited to the number of sub-apertures present in the SHWFS arrangement.
2. The second approach employs an image processing method known as a Hough transformation. A Hough transformation can be used to detect otherwise unnoticeable shapes and

patterns (i.e., lines) in a noisy image.[16] In this approach, a Hough transform is used to find the lines corresponding to the irradiance bifurcation in each sub-aperture. It is known that a line consists of co-linear points (x_i, y_i) and can be parameterized by the distance of a line perpendicular to the collection of points, ρ, and the angle, θ, at which ρ is defined, when considering the usual parameterization of a line, $\rho = x\cos(\theta) + y\sin(\theta)$. If θ is confined to an interval, say [0, 90 deg], then each parameterization is unique. However, if a line is parameterized by x_i and y_i instead of ρ and θ, the line can be identified as a set of co-linear points (ρ_i, θ_i), in the parameter space. In other words, a point in the image space corresponds to a line in the parameter space, and a point in the parameter space corresponds to a line in the image space. For the shock angle calculation, individual images of each affected sub-aperture irradiance pattern are first processed to isolate the irradiance peaks. Next, the points are transformed into the parameter space where they are represented as a group of lines. The point in the parameter space where the greatest number of lines intersect defines the ρ and θ of the hidden line in the image space. Since the θ determined through the Hough transform is defined as the angle of the line perpendicular to the line of interest and the irradiance peak bifurcation occurs orthogonal to the shock, the angle extracted from the transform is the angle of the shock. This method calculates the angle of the shock on a sub-aperture by sub-aperture basis and its accuracy is limited by the number of pixels corresponding to each sub-aperture. This approach allows for shock-tolerant phase reconstruction even if multiple shocks are present across the measurement pupil.

2.4 Improve Tilt Estimation Using Irradiance Patterns in Affected Sub-Apertures

This section discusses how the resulting irradiance patterns of the sub-apertures affected by the shock can be used to improve the local tilt information. In Ref. 10, it had been shown that the degree of irradiance pattern bifurcation is related to the pupil-plane $|\Delta\phi|$. To investigate this, phase discontinuities of varying strengths ranging from $-\pi$ to 0 rad in increments of 0.05π rad were simulated in the middle of a pupil and a Fresnel propagator was used to map the simulated pupil-plane phase to observation-plane irradiance patterns. For each resultant observation-plane irradiance pattern, the amplitude of the largest peak, I_1, was divided by the amplitude of the second largest peak, I_2. These results are shown in Fig. 2 as black circle markers where the x-axis is $\Delta\phi/\pi$ and the y-axis is I_1/I_2.

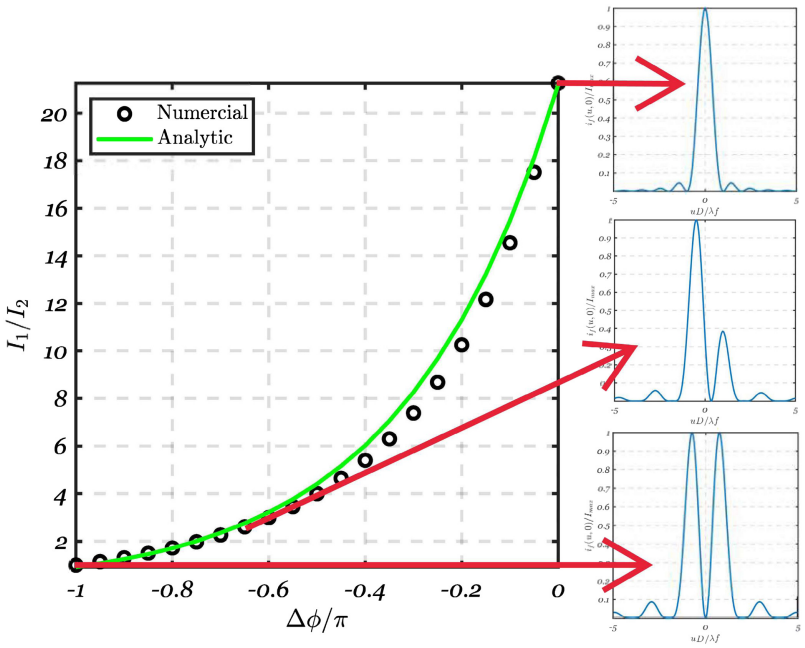

Fig. 2 Relationship between bifurcated irradiance pattern and phase discontinuity which caused it for square sub-apertures.

When there was no phase discontinuity in the pupil plane, I_1/I_2 was the diffraction-limited peak ratio for a square aperture, 21.19.[17] For this case, a one-dimensional slice of the two-dimensional irradiance pattern is presented in the top-right plot of Fig. 2. Conversely, as $|\Delta\phi|$ increases, I_1/I_2 decreases. The middle-right plot of Fig. 2 shows the one-dimensional irradiance pattern slice when a phase discontinuity of $|\Delta\phi| = 0.67\pi$ rad was imposed across the center of the pupil. Here, we see that I_2 began to increase in amplitude relative to I_1. When $|\Delta\phi| = \pi$ rad, the phase upstream versus downstream of the discontinuity was perfectly out of phase, and a bifurcated irradiance pattern with equal amplitude peaks formed, i.e., $I_1 = I_2$. This last point is shown in the bottom-right plot of Fig. 2.

Conveniently, it has been shown that for square apertures, I_1/I_2 can be related to the phase discontinuity in the pupil plane that caused the bifurcation through the following:

$$I_1/I_2 \approx 21.19 \exp(|\Delta\phi|). \tag{3}$$

In this equation, the constant is the diffraction-limited I_1/I_2 ratio for square apertures.[17] Using a fitting algorithm, an equivalent expression was found to work well for circular apertures, given as

$$I_1/I_2 \approx 26.65 \exp(|\Delta\phi|). \tag{4}$$

It is worth noting that in this expression, the constant is not the diffraction-limited I_1/I_2 ratio for circular apertures. Although these equations were arrived at heuristically, they show good agreement with the numerical results obtained using the Fresnel propagator. The results using Eq. (3) are plotted as a green line in Fig. 2. For different phase discontinuity and SHWFS conditions, such as angled shocks and experimentally collected data, a different method for relating irradiance patterns to $|\Delta\phi|$ will need to be used. However, for the purposes of this paper and for introducing the theoretical construct behind a shock-wave tolerant phase reconstructor, this analytic development will suffice, and alternative approaches continue to be explored.

It should be noted that Eqs. (3) and (4) only discern the magnitude of the phase discontinuity in the pupil-plane between 0 and π, not whether $\Delta\phi$ is positive or negative. As shown in Ref. 10, the same I_1/I_2 ratio can be accomplished when the secondary peak is on either side of the primary peak. However, it was also shown that the location of the secondary peak in relation to the primary peak is directly related to the direction of the flow for the case of an intersecting shock, as well as whether $|\Delta\phi|$ is between 0 and π or π and 2π (c.f. figure 7 in Ref. 10). For the case of a shock, the density increases across the shock and in the direction of freestream flow causing the phase of the light downstream of the shock to lag relative to the phase of the light upstream of the shock. Therefore, by knowing the direction of the flow in relation to the SHWFS measurement aperture, the true $\Delta\phi$ can be determined. For example, when the flow is moving from left to right across the measurement aperture and the secondary peak in the observation-plane irradiance pattern is to the right of the primary peak, the $\Delta\phi$ calculated from either Eq. (3) or Eq. (4) is correct. However, if the secondary peak is to the left of the primary peak, then the true $\Delta\phi$ is $2\pi - \Delta\phi$. These behaviors are flipped if the flow direction is flipped.

After using Eq. (3) or Eq. (4) in conjunction with the direction of the flow to determine the phase discontinuity across the shock for the affected sub-apertures, this information can be used to replace the tilt estimates in each sub-aperture. This is accomplished in two steps. First, the calculated change in phase across the discontinuity is converted to a change in OPD using the relation, $\Delta\text{OPD} = (-\lambda/2\pi) * \Delta\phi$, which is then used to calculate the overall tilt, θ, caused by and orthogonal to the shock using

$$\theta = \tan^{-1}\left(\frac{\Delta\text{OPD}}{D}\right). \tag{5}$$

Next, the x and y components of the corrected tilt are calculated as

$$\theta_x = \bar{\theta}_x + \theta \cos\left[\frac{(\alpha)\pi}{180}\right], \tag{6}$$

and

$$\theta_y = \bar{\theta}_y + \theta \sin\left[\frac{(\alpha)\pi}{180}\right], \tag{7}$$

where $\bar{\theta}_x$ and $\bar{\theta}_y$ are the global tilts and α is the shock wave angle in degrees. Here, the shock wave angle is calculated such that a horizontal shock is considered $\alpha = 90$ deg and a vertical shock is considered $\alpha = 0$ deg. $\bar{\theta}_x$ and $\bar{\theta}_y$ are calculated by averaging all x and y local tilts from the traditional approach, respectively.

2.5 Replace and Reconstruct

After calculation of the improved x and y tilts for sub-apertures affected by an intersecting shock from Eqs. (6) and (7), this new tilt information is then used to replace the corrupted x and y tilt values found using the traditional approach. It is important to note that the tilt estimates for the unaffected sub-apertures remain unchanged. After this replacement is made, a least-squares reconstruction is applied.

3 Results

The following sections present the results of employing the algorithm described above on both simulated as well as experimentally collected data.

3.1 Simulated Data

In this section, three simple scenarios were simulated for both square and circular sub-aperture geometries to demonstrate the shock-tolerant approach outlined above. For the results that follow, a phase discontinuity was generated and varied from 0 to 2π rad in increments of 0.05π. For simplicity, it was assumed that the SHWFS sub-apertures were illuminated by unit-amplitude, collimated light. Furthermore, it was also assumed that the shock intersects the measurement aperture at $\alpha = 0$ deg (perpendicular to the x axis) and is located in the middle of a column of sub-apertures. All scenarios outlined in this section follow the procedure described in Ref. 18. The first scenario divided the measurement aperture into a 16×16 grid of sub-apertures each with diameter $D = 6.25$ cm. The second scenario used 32×32 sub-apertures each with diameter $D = 3.125$ cm. The third scenario used 64×64 sub-apertures each with diameter $D = 1.5625$ cm. The entire grid size for each scenario was maintained at 2048×2048 grid points. For each case, a thin-lens transmittance function was then applied to each sub-aperture, and angular-spectrum propagation was used to obtain an irradiance pattern at focus. These conditions were simulated for both square and circular SHWFS lenslet shapes.

After generating simulated SHWFS frames for various $\Delta\phi$, multiple thresholding steps were taken to ensure minimal contamination from ambient light and diffraction inside the SHWFS sub-aperture locations. Next, both traditional and shock-tolerant approaches were used to generate x and y tilt matrices. The resulting tilts calculated using both approaches were then used in a least-squares reconstructor, in this case using the Southwell geometry,[3] to obtain a continuous OPD. The reconstructed OPD was then used to estimate the continuous ϕ from which $\Delta\phi$ was calculated by subtracting the phase values on either side of the shock ($\Delta\phi = \phi_{\text{DOWNSTREAM}} - \phi_{\text{UPSTREAM}}$) for both the traditional and modified approaches.

Figure 3 presents the $\Delta\phi$ results of the traditional and shock-tolerant approaches plotted as blue circle and red square markers, respectively. Here, the x axes are the input $\Delta\phi/\pi$ of the created phase discontinuities and the y axes are the output $\Delta\phi/\pi$ resulting from reconstructing the tilt values obtained using the traditional and modified approaches. Also plotted are black, dashed lines that represent the expected $\Delta\phi/\pi$. The top row of Fig. 3 presents the results obtained using square sub-apertures and the bottom row presents the results obtained using circular sub-apertures. Each column presents results obtained using a different number of sub-apertures. Specifically, the 16×16, 32×32, and 64×64 sub-aperture results are presented in columns from left to right, respectively.

As mentioned earlier and described in Ref. 10, when the $|\Delta\phi|$ induced by the shock wave becomes greater than 0.5π, the traditional phase reconstruction begins to underestimate the true $\Delta\phi$ across the shock. This is evident for all cases presented in Fig. 3. When the shock-tolerant reconstruction algorithm was employed, we see that across all cases, the reconstructed $\Delta\phi$ is in

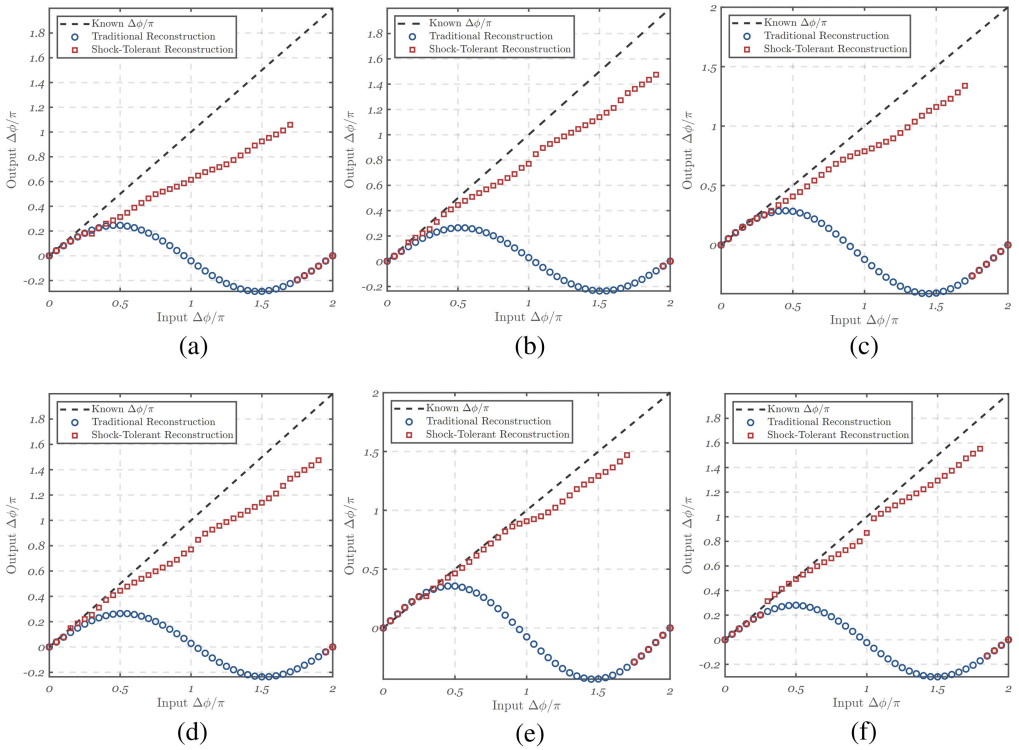

Fig. 3 Reconstructed $\Delta\phi/\pi$ compared to input $\Delta\phi/\pi$ for the traditional and shock-tolerant reconstruction approaches using simulated SHWFS imagery with (a) 16×16 square sub-apertures, (b) 32×32 square sub-apertures, (c) 64×64 square sub-apertures, (d) 16×16 circular sub-apertures, (e) 32×32 circular sub-apertures, and (f) 64×64 circular sub-apertures.

better agreement with the true $\Delta\phi$. Furthermore, the results presented in Fig. 3 also reveal that as the number of sub-apertures increase, both the shock-tolerant and traditional least-squares reconstruction algorithms deliver better estimations of $\Delta\phi$, in their own regard. With more sub-apertures, there is more local tilt information available and least-square fitting error is minimized.

The sinusoidal behavior of the traditional method, shown in blue circles in Fig. 3, is a direct result of the observation-plane irradiance pattern bifurcation. When this bifurcation increases, the irradiance pattern centroid deflection and the corresponding pupil-plane tilt are no longer in agreement for shock-affected sub-apertures. Rather, the energy associated with the pupil-plane phase discontinuity leads to beam spreading in the observation plane. For the case of a shock-wave-induced phase discontinuity, the beam spreading is predictable, as shown in Sec. 2.4. When the modified approach described above was employed, which leverages the predictability of the shock-induced observation-plane irradiance pattern beam spread, the reconstructed $\Delta\phi/\pi$ was in fair agreement with the input $\Delta\phi/\pi$ until $\Delta\phi/\pi \approx 1.8$, depending on the sub-aperture geometry. Above $\Delta\phi/\pi \approx 1.8$, the $D4\sigma$ thresholding algorithm cannot discern which sub-aperture irradiance patterns are affected by the shock due to low beam spread. Therefore, the x and y tilt values calculated using the traditional approach are used instead.

3.2 Experimental Data

This section demonstrates the shock-tolerant phase reconstruction algorithm on experimentally collected SHWFS imagery. In order to acquire the experimental data, a 532 nm laser source was first linearly polarized using a $\lambda/4$ wave-plate, expanded, and collimated. The beam was then reflected off a spatial-light modulator (SLM). The SLM was used to impart phase discontinuities ranging from 0 to 2π rad in increments of 0.05π rad at a 0 deg angle in the middle of the beam. In combination with an iris and collimating lens after the SLM, a focus and tilt term were also applied to the SLM in order to decouple the zeroth-order diffractive term from the first-order diffractive term which contains the applied phase information. After which, the beam was

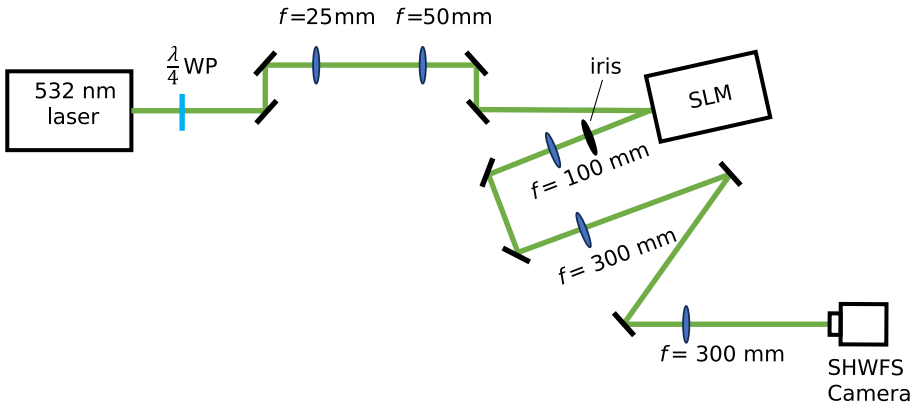

Fig. 4 Experimental setup for the SHWFS data collection (not drawn to scale).

re-imaged onto an SHWFS using a $4f$ relay consisting of two 300 mm lenses. A schematic of this experimental setup is presented in Fig. 4.

The SHWFS used 18×18 square, sub-apertures with a diameter of $D = 0.148$ mm and a focal length of $f = 6.7$ mm. The detector screen size was 360×360 pixels, so each lenslet was comprised of 20×20 pixels. The beam-spread threshold used for this data was $D4\sigma/D_{\mathrm{DL}} = 2.9$. Figure 5 shows the resultant SHWFS imagery for phase discontinuities of 0, $\pi/2$, and π as well as the sub-apertures that qualify, which are highlighted by red squares.

Due to realistic experimental factors such as non-uniform pupil illumination and camera measurement noise, Eq. (3) could not be used to estimate the shock-induced $\Delta\phi$ from the ratio of bifurcated irradiance pattern peaks. Instead, another equation was developed using a fitting algorithm to empirically collected data. After which, the experimental SHWFS measurements were processed using the traditional and shock-tolerant reconstruction approaches. These results are presented in Fig. 6.

Here, it can be seen that the traditional reconstruction results exhibit the same behavior observed in Fig. 3 as well as in Ref. 10. Furthermore, we see that the shock-tolerant reconstruction results presented in Fig. 6 are in fair agreement with the results presented in the top-right plot of Fig. 3, where the number of sub-apertures was comparable to the number of sub-apertures used in the experiment. We expect that if the number of sub-apertures increased, the $\Delta\phi$ measured after employing the shock-tolerant reconstruction algorithm would likely be closer to the expected $\Delta\phi$. It is also worth noting that for $\Delta\phi/\pi$ values close to 1.35, the shock-tolerant reconstructed $\Delta\phi/\pi$ begins to level off. This is a result of the Gaussian beam used for the experiment. At $\Delta\phi/\pi$ values where the beam spread is low, the algorithm cannot discern between affected and unaffected sub-apertures based on the observation-plane irradiance pattern. This is especially true for those lenslets that lie close to the edge of the beam. The non-uniform illumination caused by the Gaussian beam profile leads to fewer detections of sub-apertures affected by the shock and consequently, more fitting error in the least-squares reconstruction. Nonetheless, the

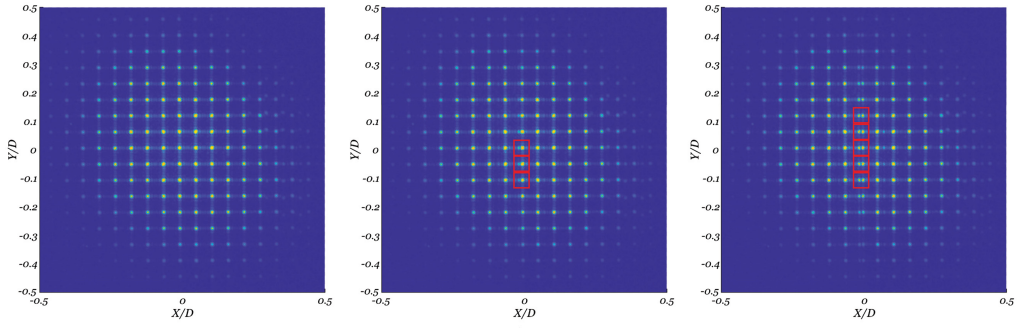

Fig. 5 Experimentally collected SHWFS imagery for (a) $\Delta\phi = 0$ rad, (b) $\Delta\phi = \pi/2$ rad, (c) $\Delta\phi = \pi$ rad phase discontinuities.

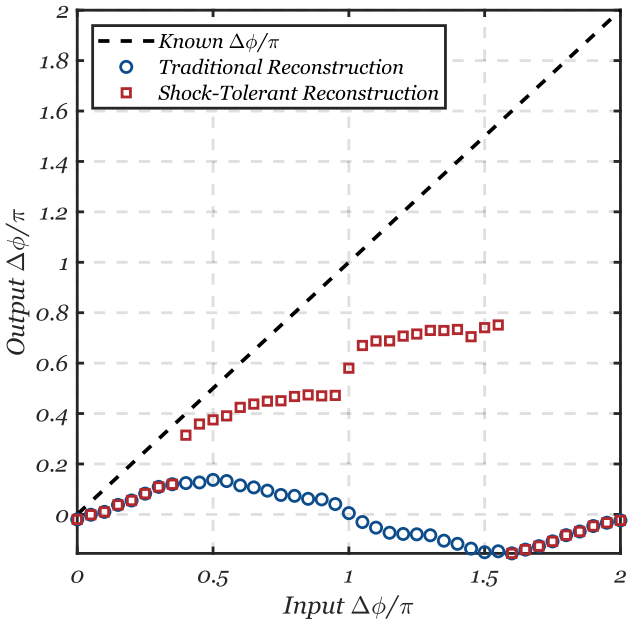

Fig. 6 Reconstructed $\Delta\phi/\pi$ compared to input $\Delta\phi/\pi$ for the traditional and shock-tolerant reconstruction approaches using experimentally collected SHWFS imagery.

shock-tolerant algorithm is in fair agreement with the known $\Delta\phi$ until $\Delta\phi \approx 1.6\pi$ rad, where past this, the traditionally collected x and y tilt values were used.

4 Conclusions

This paper utilized recent developments which described the effects of shock-induced, phase discontinuities on SHWFS measurements to introduce an SHWFS-based, shock-tolerant phase reconstruction algorithm. This algorithm first thresholds the beam spread calculated for each SHWFS irradiance pattern to identify sub-apertures affected by the shock. The shock-affected SHWFS irradiance patterns were then used to obtain a better estimate of the local tilt across the sub-aperture pupils. The corrupted tilt information was replaced with these improved tilt estimates and reconstructed. This algorithm was demonstrated on both simulated as well as experimental data obtained using an SLM. The results presented in Figs. 3 and 6 demonstrate that with the extensions presented in this paper, we can improve SHWFS-based wavefront sensing when phase discontinuities are present across the measurement pupil. The promising developments presented here will enable robust wavefront sensing in transonic, supersonic, and hypersonic environments using an SHWFS.

Disclosures

The authors declare no conflicts of interest.

Code and Data Availability

Data underlying the results presented in this paper are not publicly available at this time but may be obtained from the authors upon reasonable request.

Acknowledgments

The authors would like to thank the Joint Directed Energy Transition Office (JDETO) as well as the Air Force Research Lab Scholars Program for sponsoring this work. The authors would also like to thank NSWCDD's NISE Adaptive-Optics Testbed effort for providing the experimental facilities used to collect the data presented in this paper. Distribution Statement A. Approved for public release: distribution is unlimited. Public Affairs release approval #: AFRL-2023-3830.

References

1. D. Fried, "Least-square fitting a wave-front distortion estimate to an array of phase-difference measurements," *J. Opt. Soc. Am.* **67**, 370–375 (1977).
2. R. Hudgin, "Wave-front reconstruction for compensated imaging," *J. Opt. Soc. Am.* **67**, 375–378 (1977).
3. W. Southwell, "Wave-front estimation from wave-front slope measurements," *J. Opt. Soc. Am.* **70**(8), 998–1006 (1980).
4. D. L. Fried, "Branch point problem in adaptive optics," *J. Opt. Soc. Am.* **15**, 2759 (1998).
5. T. Brennan, "Estimation of atmospheric parameters from the slope discrepancy," tech. rep., The Optical Sciences Company (2003).
6. M. Kalensky, "Branch-point identification using second-moment Shack–Hartmann wavefront sensor statistics," *Appl. Opt.* **62**, G101–G111 (2023).
7. M. Kalensky et al., "Comparison of branch-point detection approaches using a Shack–Hartmann wavefront sensor," *Opt. Eng.* **62**(12), 123101 (2023).
8. T. E. DeFoor et al., "Shock-wave tolerant phase reconstructor for the Shack–Hartmann wavefront sensor," *Proc. SPIE* **12694**, 126930R (2023).
9. M. Kalensky, M. R. Kemnetz, and M. F. Spencer, "Effects of shock-related discontinuities on shwfs measurements: modeling and simulation," *Proc. SPIE* **12239**, 122390J (2022).
10. M. Kalensky, M. R. Kemnetz, and M. F. Spencer, "Effects of shock waves on Shack–Hartmann wavefront sensor data," *AIAA J.* **61**, 1–13 (2023).
11. J. Panda and G. Adamovsky, "Laser light scattering by shock waves," *Phys. Fluids* **7**, 2271–2279 (1995).
12. M. R. Kemnetz et al., "Effects of shock-related discontinuities on SHWFS measurements: experimental results," *Proc. SPIE* **12239**, 122390I (2022).
13. J. Morrida et al., "Shock-related effects on aero-optical environment for hemisphere-on-cylinder turrets at transonic speeds," *Appl. Opt.* **56**, 4814 (2017).
14. A. E. Siegman, "How to (maybe) measure laser beam quality," in *DPSS (Diode Pumped Solid State) Lasers: Appl. and Issues*, OSA (1998).
15. K. Tikuišis, "peaks2 - find peaks in 2D data without additional toolbox," MATLAB Central File Exchange (2023).
16. R. O. Duda and P. E. Hart, "Use of the hough transformation to detect lines and curves in pictures," *Commun. ACM* **15**, 11–15 (1972).
17. J. Goodman, *Introduction to Fourier optics*, Roberts & Co, Englewood, Colorado (2005).
18. M. Kalensky et al., "Estimation of atmospheric optical turbulence strength in realistic airborne environments," *Appl. Opt.* **61**, 6268 (2022).

Thomas E. DeFoor is an undergraduate senior student at The Ohio State University in Columbus, Ohio. He is pursuing an engineering physics degree with a specialization in aerospace engineering with plans of graduating in May of 2024. In addition, he was a directed energy intern through the Air Force Research Lab (AFRL) Scholars Program at Kirtland AFB in Albuquerque, New Mexico, as a part of the Universities Space Research Association.

Matthew Kalensky is an engineer at the Naval Surface Warfare Center Dahlgren Division. He received his BS degree in mechanical and materials engineering from Loyola University Maryland in 2017 and his MS and PhD degrees in aerospace engineering from the University of Notre Dame in 2020 and 2022, respectively. He actively runs a cross-service adaptive-optics working group, is a chair for the Unconventional Imaging, Sensing, and Adaptive Optics conference at SPIE Optics and Photonics, and is the webinar officer for Optica's Laser System's Technical Group. His expertise and research interests are in beam control, deep-turbulence characterization, and aero effects.

Matthew R. Kemnetz is the principal investigator of the Laser Beam Control (formerly Aero-Effects and Beam Control) Program at the Air Force Research Laboratory Directed Energy Directorate, AFRL/RDLTS. He came to the Air Force after graduating from the University of Notre Dame in 2019 with his PhD in aerospace and mechanical engineering. His dissertation work focused on aero-effects in directed energy. More specifically, the dissertation produced a novel algorithm for first ever direct experimental measurements of aero-optical jitter. For the Air Force, he leads the Aero-Effects Laboratory at Kirtland Air Force Base. In addition, he manages a diverse research portfolio across aero-effects, beam control, and atmospheric propagation.

Timothy J. Bukowski is a current graduate student in the Aero-Optics group at the University of Notre Dame. Here, he works on many problems related to laser propagation systems. He has also

worked as an SSEP intern at the Naval Surface Warfare Center Dahlgren Division within the Integrated Engagement Systems Department and the Optics and Beam Control Branch, where he worked on problems related to beam propagation through distributed-volume turbulence. He is an Arthur J. Schmitt Leadership Fellow and was recently awarded the NDSEG fellowship.

Mark F. Spencer is the director of the Joint Directed Energy Transition Office within the Office of the Under Secretary of Defense for Research and Engineering. He is also an adjunct associate professor of optical sciences and engineering at the Air Force Institute of Technology within the Department of Engineering Physics. He is a fellow of SPIE.